Construction and Building Materials 430 (2024) 136439

Contents lists available at ScienceDirect

Construction and Building Materials

journal homepage: www.elsevier.com/locate/conbuildmat

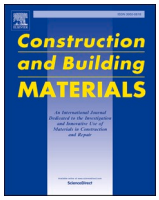

Printhead mixing of geopolymer and OPC slurries for hybrid alkali-activated cement in 3D concrete printing

Sayanthan Ramakrishnan [a,b,*], Kirubajiny Pasupathy [a], Viktor Mechtcherine [c], Jay Sanjayan [b]

[a] Centre for Future Materials, School of Engineering, University of Southern Queensland, Springfield, QLD 4300, Australia
[b] Centre for Sustainable Infrastructure and Digital Construction, School of Engineering, Swinburne University of Technology, Hawthorn, Victoria 3122, Australia
[c] Institute for Construction Materials, TU Dresden, Dresden, Germany

ARTICLE INFO

Keywords:
Concrete 3D printing
Hybrid alkali cement
Set-on-demand
Rheology
Geopolymer

ABSTRACT

Hybrid alkali cement (HAC) is regarded as a sustainable alternative to cementitious materials due to the use of more than 70 % of supplementary cementitious materials while the issues associated with geopolymers are avoided to a great extent. This paper proposes a new method of delivering HAC-based mixtures by a two-part printhead mixing process suited for 3D concrete printing (3DCP). The two-part mixing process addresses the conflicting rheological requirements in 3DCP by facilitating the rapid early-age strength development after placement while showing excellent pumpability prior to the extrusion. The proposed approach is based on introducing the Portland cement in a secondary mixing process to partially replace the fly ash or slag in the printable geopolymer mix. A series of experiments assessing the printability of fresh concrete following the two-part mixing process and the properties of hardened concrete were assessed. The results demonstrate that the replacement of FA with Portland cement (HAC-FA) yielded a more pronounced enhancement than slag-replaced mixes (HAC-S) with the increase in static yield stress (SYS) and modulus of elasticity by 17 times and 3.5 times respectively at 30 min, compared to the control mix. The hardened properties of printable mixes, namely compressive strength and interlayer bond strength at 28 days, revealed an enhancement for the HAC-25FA mix by 20 % and 64 %, respectively, again in comparison to the control mix. The apparent volume of permeable voids (AVPV) and microstructural analysis validated the hardened concrete properties, where the HAC-FA mixes showed the densest microstructure with a reduced apparent porosity, compared to other mixes.

1. Introduction

Digital construction methods using 3D concrete printing (3DCP) technology have significantly evolved in the past two decades, thanks to the dedicated research and development conducted by researchers and industrial practitioners around the world [1–3]. The driving forces for the significant development of this emerging technology are its automated manufacturing process, formwork-free construction, architectural freedom allowing the construction of intricate structures and increased productivity [4]. The extrusion-based 3DCP is commonly referred to as a feasible method for large-scale digital construction, wherein the concrete is deposited as discrete layers extruded through a nozzle [5]. The nozzle shape and size determine the geometry of the filament and hence, the features of printed elements. As the 3DCP construction process largely differs from the traditional formwork casting technology, it comes with specific challenges for industrial implementation. The challenges of 3DCP, compared to traditional formwork casting method, are identified as anisotropic mechanical behaviour [6], poor interlayer adhesion [7], uneven surface quality [8], strict rheological requirements [9,10] and various modes of possible failure/collapse [11,12]. Among these challenges, the strict rheological requirements associated with the low viscosity and yield stress during the pumping and extrusion stages followed by a rapid transition to a pseudo-solid state after deposition remain a major one.

The most commonly studied method to meet the above-stated rheological requirements is by a chemical intervention, where the set accelerators are introduced at the printhead followed by a short-duration mixing process [13]. Immediately after the mixing process, the accelerator would enable the fast stiffening and setting of printable cementitious materials, thus allowing the transition of printable mixes from a viscoelastic state to a pseudo-solid state. The concept of introducing accelerators in printhead was studied by Esnault et al. [14] by

* Corresponding author at: Centre for Future Materials, School of Engineering, University of Southern Queensland, Springfield, QLD 4300, Australia.
E-mail address: saya.ramakrishnan@usq.edu.au (S. Ramakrishnan).

https://doi.org/10.1016/j.conbuildmat.2024.136439
Received 17 December 2023; Received in revised form 12 April 2024; Accepted 26 April 2024
Available online 8 May 2024

incorporating an alkali-free shotcrete accelerator in the extrusion nozzle. The authors found that the mixes containing the accelerator showed a failure stress of 82.7 kPa and 179 kPa at 15 min and 30 min respectively, compared to 13.1 kPa and 25.3 kPa for a mix incorporating viscosity modifying admixture (VMA). In another study [6,15], the accelerating additive injection at a dosage of 3 % and 6 % showed average strength and stiffness enhancement by 107 % and 108 % respectively for 3 % and 155 % and 177 % respectively for 6 %. The authors concluded that the accelerator injection is a feasible way to improve the design freedom of print objects. Gosselin et al. [16] demonstrated large-scale printing using ultra-high performance concrete by introducing the accelerator at the printhead. The novel premix consisting of Portland cement, crystalline silica, silica fume and limestone powder showed the feasibility of producing large-scale printed structures without temporary supports.

While the chemical intervention with the introduction of set-accelerators at the printhead has undergone significant developments, these advancements do not address the sustainably issues related to the use of cement. Portland cement has been identified as a major contributor to environmental pollution with approximately 8 % of global carbon emissions being caused by its production [17–20]. To resolve this concern, alkali-activated cements and geopolymers have been identified as sustainable alternatives to Portland cement-based binders. For such materials, industrial by-products which are rich in alumina and silica are used as cement replacements. Their reactions with alkali activators result in the formation of 3-dimensional networks of SiO_4 and AlO_4 with excellent mechanical, thermal and durability properties [21]. Geopolymers are reported to reduce the carbon emission of Portland cement-based concrete by up to 80 % [22]. Considering these sustainability merits, the geopolymer concretes for 3DCP applications have also been studied. In particular, the inline activation of geopolymers to meet the conflicting rheological requirements for 3DCP has been studied by researchers [10,23,24]. The geopolymers allow introducing the activators to the precursor slurry at the printhead for immediate geopolymerisation process. This is advantageous as the precursor slurry remains inactive for a long period without the use of any retarders. The authors have reported that the inline activation of geopolymer slurry at the printhead will reach the static yield stress (SYS) of 70 kPa in 20 min [24]. In addition, authors have demonstrated the feasibility of printing out of plane elements without the support. While the concept of inline activation of geopolymers is similar to the accelerator injection at the printhead, it significantly differs in terms of the mixing requirements. This is primarily due to the ratio of two parts in the printhead mixing process. For accelerator injection, a small dosage of accelerator is mixed at the printhead, while in geopolymer systems, the activators are of a comparably high amount, so that significantly higher mixing energy is required to attain a homogenous mixture. Moreover, uniform mixing of activators and precursors is crucial in geopolymers since inadequate mixing will lead to non-uniform distribution of alkali ions in the precursors that could result in weak geopolymer matrix. The geopolymer printhead mixing is generally classified as two-part mixing process due to the comparable ratio of two parts of mixes (i.e., precursor slurry and activator slurry). Similar printhead mixing process was also conducted by Tao et al. [6,25] for cementitious systems, where the liquid accelerator dosing was replaced by a carrier fluid containing the necessary admixtures. The authors claimed that the carrier fluid system has many benefits compared to the accelerator dosing process such as similar viscosity of two streams providing better mixing homogeneity. Furthermore, the carrier fluid dilutes the accelerator concentration at the inlet and the risk of inlet blockage due to rapid stiffening can be reduced [26]. This strategy is called a twin-pipe pumping process. The authors showed the feasibility of printing up to a height of 3 m of structure in 9 min using the twin-pipe pumping strategy [27].

Even though geopolymer concrete has significant sustainability merits and waste utilisation benefits, it also has many issues when it comes to industrial applications. The major issues are high shrinkage, efflorescence formation that could lead to an unpleasant appearance and the potential alkali-silica reactions [28]. In 3DCP applications, the absence of formwork could further exacerbate the shrinkage that could lead to surface cracking and affect the long-term durability performance. To solve these issues while retaining the sustainability and waste utilisation benefits, a novel binder material, namely hybrid alkali-activated cement (HAC) [29] – was recently proposed by introducing a small amount of OPC into alkali-activated supplementary cementitious materials. HAC has many merits over geopolymer binders such as more compact and denser microstructure due to the presence of both geopolymer and C-S-H gels. The production of HAC is not difficult compared to geopolymers along with the evidence suggesting the commercial manufacture of hybrid cements, especially in a cement plant in America [30–33]. Apart from the significant merits of HAC for traditional construction practice, this binder possesses a special advantage for the 3DCP application which is inline activation of HAC to meet the conflicting rheological requirements. More precisely, the mixing of a small amount of OPC into the alkali activated supplementary cementitious materials (SCMs) will result in the rapid setting of concrete due to the reaction between calcium ions in OPC and alkali ions. This can be advantageous for 3DCP, where the OPC can be introduced at the printhead for a premixed SCM-alkali activator slurry to attain rapid SYS development. Moreover, the dosage of OPC can be chosen to achieve the desired SYS growth rate as required for the applications.

Considering the abovementioned benefits of HAC in emerging 3DCP applications, this study intends to develop 3D printable HAC by two-part printhead mixing strategy. Here, the two parts are considered as SCM-activator slurry and OPC slurry. As per the authors' best knowledge, there are no known studies investigating the printhead mixing strategy of HAC for the on-demand setting of concrete. The HAC mixes are developed by partial replacement of fly ash and slag with OPC at the replacement levels of 12.5 % and 25 % by mass. The fresh rheological properties of printable mixes, including the static yield stress growth, elastic modulus, apparent viscosity recovery and flowability properties are assessed. The hardened properties of HAC-based 3DCP specimens are compared with the geopolymer printed specimens as well as mould-cast specimens. Finally, the microstructural analysis is conducted to better understand the variation in hardened properties of 3D printed concrete and to evaluate the effect of OPC on the microstructure of HACs.

2. Experimental methodology

2.1. Materials

The general-purpose (Type GP) Portland cement, ground granulated blast furnace slag (hereafter called slag) and low-calcium fly ash (class F) were used to formulate the binder composition in this study. Both slag and fly ash comply with Australian standard AS 3582.1 [34] and OPC complies with Australian standard AS 3972 [35]. Two grades of silica sands, denoted as coarse sand and fine sand, were used. The median diameter (D50) of the fine sand and coarse sand were 172 μm and 498 μm, respectively. Sodium metasilicate (Na_2SiO_3) anhydrous powder ($SiO_2/Na_2O = 1.0$), supplied by Redox Pty Ltd- Australia, was used as a solid activator for the geopolymer preparation. In addition, sucrose powder at 1 wt % of the binders was used as a retarder to increase the open time of geopolymer slurry. Sucrose has been widely used as a retarder in geopolymers 3D printing applications [36,37].

2.2. Sample preparation and printing process

The mix composition of control and HAC mixes are given in Table 1. Here, the HAC mixes are designated by slag and fly ash replacement with OPC with the maximum replacement levels of 25 wt % of the binders. The total water-to-precursor ratio was kept at 0.4 for the mixes G and HAC-12.5FA. For the remaining mixes, the water-to-precursor ratio was

Table 1
Mix compositions of HAC mixes for 3DCP.

Group Details	Geopolymer slurry								OPC slurry		
	Mix ID	Slag (kg)	Fly ash (kg)	Coarse Sand (kg)	Fine Sand (kg)	Na_2SiO_3 (kg)	Water (kg)	Retarder (% of binder)	OPC (kg)	Water (kg)	Total water/ precursor ratio
Control	G	0.5	0.5	1	0.5	0.1	0.400	1	0	0	0.4
HAC-FA	HAC-12.5FA	0.5	0.375	1	0.5	0.1	0.35	1	0.125	0.05	0.4
	HAC-25FA	0.5	0.25	1	0.5	0.1	0.315	1	0.25	0.105	0.42
HAC-S	HAC-12.5 S	0.375	0.5	1	0.5	0.1	0.368	1	0.125	0.052	0.42
	HAC-25S	0.25	0.5	1	0.5	0.1	0.315	1	0.25	0.105	0.42

adjusted to 0.42 to attain the required extrudability properties. Fine sand-to-binder and coarse sand-to-binder ratio were chosen as 0.5 and 1, respectively. The total amount of activator was kept constant for all mixes at 10 % of total precursor content.

The mixing process was designed to represent a two-part mixing system with one part of the mix containing the geopolymer slurry and the second part being OPC slurry. The ideal two-part mixing process with an in-line dynamic mixer at the print head is schematically illustrated in Fig. 1. However, for this study, the two-part mixing process was conducted by mixing two components in the Hobart mixer as described below. For the first part preparation, the dry ingredients of slag, fly ash, two types of sand and sodium metasilicate were mixed in a Hobart mixer at the slow speed of 61 RPM for 3 min. Following the homogenous dry mixing, 85 % of the necessary amounts of water and retarder were added, and the mixing process was continued for 10 min at a medium speed (121 RPM). Subsequently, the remaining water was added to the mixture, and the mixing was continued for another 5 min at the same speed. It is important to highlight that the wet mixing was conducted for a total of 15 min to allow sufficient time for the dissolution of sodium metasilicate, as reported previously [38]. The produced geopolymer wet mix represents the first of the two-part mixes. Meanwhile, the second part of the mix was prepared by mixing OPC and required water in another Hobart mixer for 3 min at a slow speed (61 RPM) to attain a pumpable OPC slurry. Thereafter, the two parts of the wet mixes were mixed for a short duration of 30 s to represent the printhead mixing process.

Once both parts of the slurries are mixed for a short duration, the wet mix was immediately transferred to the extruder head of the 3D printer for printing purposes. The wet mix was also poured into 50 $\times$50$\times$50 mm^3 steel cubic moulds for the testing of mould-cast specimens. To conduct the 3D printing processes, a custom-made piston-mounted ram extruder with a length of 350 mm and a diameter of 50 mm was used. A 40 mm (W) x 20 mm (H) rectangular nozzle was attached to the opening of the extruder. Soon after the two-part mixing process, the fresh printable mix was filled into the extruder and the extrusion was performed at the speed of 10 mm/s. The samples were printed with the dimensions of each layer at 40 mm (Width) $\times$ 20 mm (Height) $\times$ 300 mm (Length). The printed filaments were kept in the thermally controlled environmental chamber operated at 25°C and 50 % relative humidity until the fresh properties' measurements. For hardened properties assessment, the printed and mould-cast specimens were covered by a plastic film for 24 h to avoid the surface moisture loss. After 24 h, the samples were transferred to a water bath curing until the test date.

3. Experimental programme

3.1. Evaluation of static yield stress development with time

The purpose of the two-part mixing at the printhead is to attain rapid early-age strength development of concrete just after placement. The early age strength development can be experimentally assessed by using various methods such as uniaxial compression test of the extruded concrete, rheological tests, slow penetration test, conducting print trials until failure etc. Chang et al. [39] provide an extensive review of these methods for 3DCP. Among these test methods, the slow penetration method, proposed by Looten et al. [39], has been widely used for printable mixes due to the merits of continuous measurement of static yield stress with time, minimal disturbance to the sample, quasi-static measurement due to slow penetration and direct conversion to SYS. Therefore, this study uses a slow penetration test to assess the static yield stress (SYS) of printable mixes just after the two-part mixing process.

The slow penetration test measures the resistance to the penetration of a conical head into the concrete mix at a slow rate. Fig. 2 illustrates the experimental setup of the test. The specification of the conical head is 30 mm in height and 20 mm in diameter, which is attached to a 500 N-load cell and the mechanical testing system (MTS). The

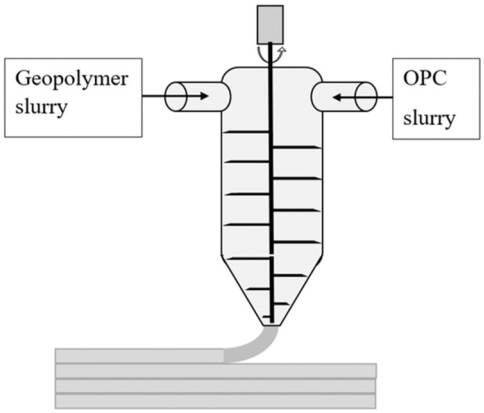

Fig. 1. Schematic diagram of an ideal two-part printhead mixing process.

Fig. 2. Slow penetration test setup for SYS measurement.

penetrometer was operated at a constant speed of 10 mm/h. Based on the resistance force derived from the penetration test, the static yield strength of concrete is calculated using Eq. (1) [39]:

$$\tau = \frac{F}{\pi R\sqrt{R^2 + h^2}} \quad (1)$$

where F is the penetration resistance force measured by the load cell (N), R is the cone radius (mm), and h is the cone height (mm).

3.2. Determining the modulus of elasticity of fresh 3D-printed filaments

While the SYS development demonstrates the buildability enhancement of the HAC mixes according to the plastic collapse failure criterion, the elastic buckling failure of printed elements is governed by the stiffness of the printed filaments. Therefore, the evolution of the modulus of elasticity was determined on a 3D-printed two-filament specimen at discrete time intervals of 10, 20, 30 and 40 min after printing. The specimens were printed with a piston-type extruder with a rectangular nozzle of 40 mm×20 mm. Length of the deposited filaments was 100 mm and the time interval between the layers was one minute. The printed specimens were kept in an environmentally controlled thermal chamber operated at 25℃ and 50 % RH until the test.

The test was conducted by subjecting the 3D printed specimens to a compression loading at a displacement control mode as shown in Fig. 3. The loading was applied at 10 mm/min until the deformation reached 1 mm to limit the strain to 5 %. The compression load was measured using a highly sensitive 500 N-load cell at the data acquisition rate of 10 Hz. The modulus of elasticity of the printed specimen was determined from the slope of the linear portion of the stress-strain curve.

3.3. Setting time measurement of the fresh mix

The initial and final setting times of the 3D printable mixes after the two-part mixing process were measured to assess the effect of OPC content on the setting of HAC mixes, compared to control geopolymer concrete. The setting times measurements were conducted using a Vicat needle apparatus as per ASTM C191 standard. For this test, the prepared HAC mixes were transferred to the Vicat mould and positioned on the apparatus. The needle was initially set to the standard height of the apparatus and quickly released by pushing the release plunger. The depth of needle penetration was measured for varying time intervals from initial mixing. The time required to meet the needle penetration depth of 25 mm and 0.5 mm were recorded as initial and final setting times, respectively.

3.4. Rheological properties of the fresh mix

The two-part mixing process at the printhead involves a short duration mixing of two slurry components with the purpose of attaining rapid setting and hardening after placement. However, the mixes should have sufficient extrudability and shape retention properties just after printhead mixing process. The mixing energy is a critical factor in printhead mixing process, where excessive mixing energy may break the immediate reaction products (i.e., C-S-H and C-A-S-H gels) that could hinder the stiffening process of HAC, consequently leading to low extrudability and buildability. The mixing energy is directly proportional to the mixing duration at a given mix speed and therefore, the mixing duration should be carefully chosen to prevent the above-mentioned issues. For this purpose, a viscosity recovery assessment by following the three stage shearing protocol shown in Fig. 4 was conducted. Here, once the two-part mixing process for the specified short duration mixing (i.e., 15 s) was completed, the material was subjected to further mixing to assess re-shearing effect on the extrudability properties of 3D printable mixes. By conducting secondary shearing and assessing the viscosity properties following the additional shearing effect, the effects of excessive mixing at the printhead on the extrudability and shape retention of printable two-part mixes can be assessed. The proposed three stage shearing protocol to assess the viscosity recovery properties of printable mixes has been widely used in the past studies [40–42]. The three-stage shearing protocol follows a low shearing regime (0.01 s^{-1}) at the first stage to reflect the extrusion process followed by high shearing at 13 s^{-1} to reflect the re-shearing of the printhead mixed and concludes with the low shearing rate (0.01 s^{-1}) to understand the effects of high shearing (stage 2) on the extrudability of printable mixes.

For the viscosity recovery test, a rotational rheometer (Viskomat XL) with a six-blade vane probe accessory was employed. The radius and the height of each blade were equal to 39.5 mm and 69 mm, respectively. The radius of the vessel used for filling the fresh concrete was 82.5 mm.

3.5. Compressive strength test

The compressive strength properties of 3D printable HAC mixes were assessed to understand the effect of the cement content on the anisotropic strength development of HAC mixes. The compressive strength measurement was determined on the 3D printed samples in longitudinal, lateral, and perpendicular directions to assess the expected anisotropy. The schematic diagram of the compressive strength test of the 3D printed samples in three directions is shown in Fig. 5. To conduct the test, 40 × 40 × 40 mm^3 size samples were extracted from the printed specimens and the compressive strength test was performed at the age of 7 days and 28 days. The compressive strength of mould-cast specimens was conducted using 50 ×50 × 50 mm^3 samples in accordance with ASTM C109. The compressive strength measurements were carried out

Fig. 3. Experimental setup for measuring the modulus of elasticity.

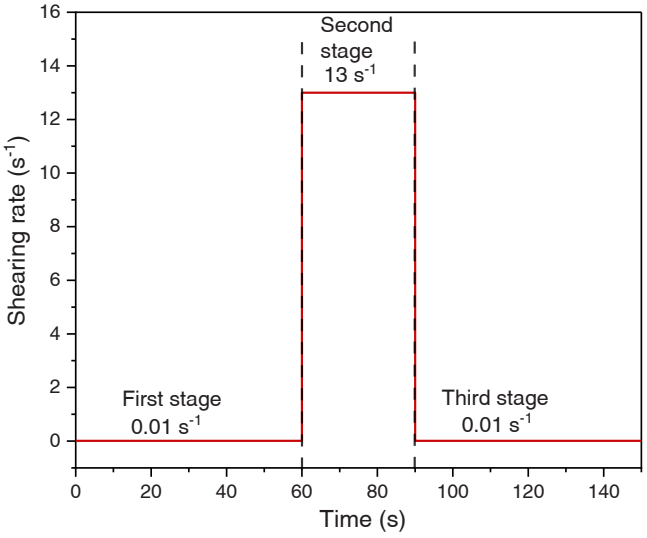

Fig. 4. Rheological testing protocols for viscosity recovery test.

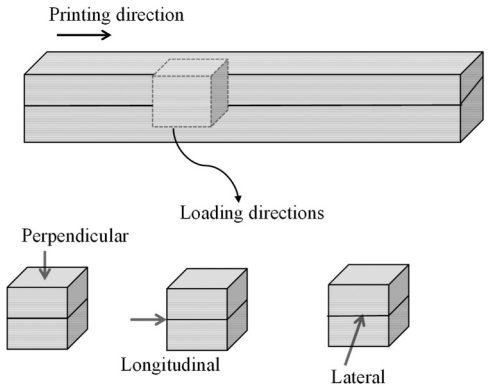

Fig. 5. Schematic diagram of samples extracted from printed samples and testing directions for compressive strength tests.

using a Universal Mechanical Testing System (MTS) with a maximum load capacity and a precision of 300 kN and 0.01 kN, respectively. The loading rate during the test was maintained constant with 0.5 kN/s.

3.6. Interlayer bond strength test

The two-part mixing of geopolymer and OPC slurries to produce the so-called HAC mixes will have a rapid setting and hardening process, which may affect the malleability and surface moisture content of the printed layers. The poor malleability and low surface moisture content can lead to reduced interlayer bond strength, which is a major concern in 3D printed specimens. Therefore, the interlayer bond strength of 3D printed specimens was determined to assess the effect of rapid early setting and hardening in the HAC mixes.

To conduct the interlayer bond strength, the samples were prepared with the dimensions of 40 ×40×40 mm^3 cubes extracted from the 3D printed specimens. The samples were first prepared by creating a triangular notch at interlayer of the specimen as shown in Fig. 6(b). A custom-made test rig, containing two metallic clamps with adjustable spacing of the clamp, is attached at the interlayer of the specimen on top and bottom layers. The clamps were connected to the universal mechanical testing system (MTS) to conduct a direct tensile strength test. The test was conducted at the displacement control mode with the rate of 0.5 mm/min. The accuracy of the MTS machine is 0.1 kN. The bond strength was determined by measuring the maximum tensile load and the effective bond area. This test method has been widely used in the past to determine the interlayer bond strength of 3D printing elements [24,43]. Three specimens were tested for each mix design and the average interlayer bond strength along with the standard deviation of the results were derived.

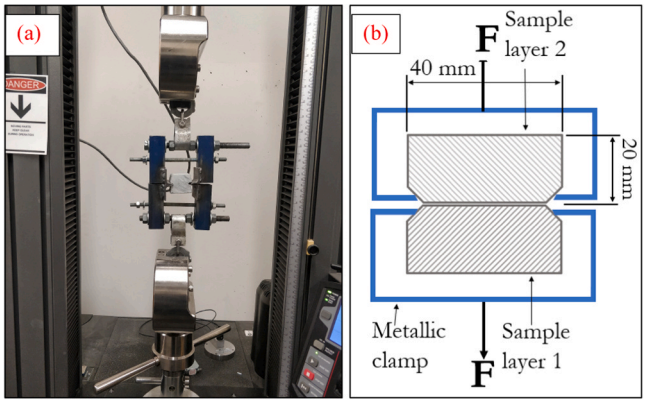

Fig. 6. Experimental setup for interlayer bond strength measurement of 3D printed samples (a) experimental set up (b) schematic diagram of the test.

3.7. Apparent volume of permeable void (AVPV) measurements

The apparent volume of permeable voids (AVPV) of 3D printed, and mould-cast HAC mixes were determined in accordance with ASTM C642 standard to assess the porosity variation among the different HAC mixes. To perform the test, three specimens from each 3D printed mix groups with the size of 40 × 40 × 40 mm^3 and three mould-cast specimens with the size of 50 × 50× 50 mm^3 were used. The experimental procedure was as follows. Initially, all samples were subjected to oven-drying process at a temperature of 105°C for 24 h, and the oven-dried mass were measured and recorded as 'A' in g. Subsequently, the samples were immersed in water for 24 h to ensure their saturation, after which they were boiled for a duration of 5 h. The mass of the boiled samples was measured and recorded as 'B' in g. After that, the suspended mass of the samples was determined as 'C' in g. The accuracy of the balance used for the measurements was 0.01 g. The AVPV (V %) was calculated using Eq. (2):

$$V = \frac{B - A}{B - C} \times 100\% \quad (2)$$

3.8. Micro-morphology analysis

The microstructural analysis of the 3D printed HAC specimens was assessed by a Scanning Electron Microscopy (SEM ZEISS Supra 40 VP). To perform the test, a 10 mm size sample was extracted from the printed specimens after 28 days. The sample was first gold coated for a thickness of 15 nm using the K975X vacuum coating system. The gold-coated specimen was then transferred to the SEM chamber operated at an accelerating voltage of 5 kV with a working distance (WD) of ~ 20 mm. One sample was tested for each mix design group.

4. Results and discussion

4.1. Static yield stress development with time

Fig. 7 shows the SYS development of control and various HAC mixes determined using the slow penetration test. Here, the SYS measurements were taken at a frequency of 4 Hz. Among the mixes considered, the control geopolymer mix (G) showed the lowest yield stress throughout the test duration. For instance, the measured static yield stress of G at 10 min and 30 min was 4.6 kPa and 10.2 kPa, respectively. The significantly low yield strength of this mix is due to the retarder in the mix which inhibits the geopolymerisation process. On the other hand, the HAC mixes containing OPC as a replacement for slag or FA showed rapid

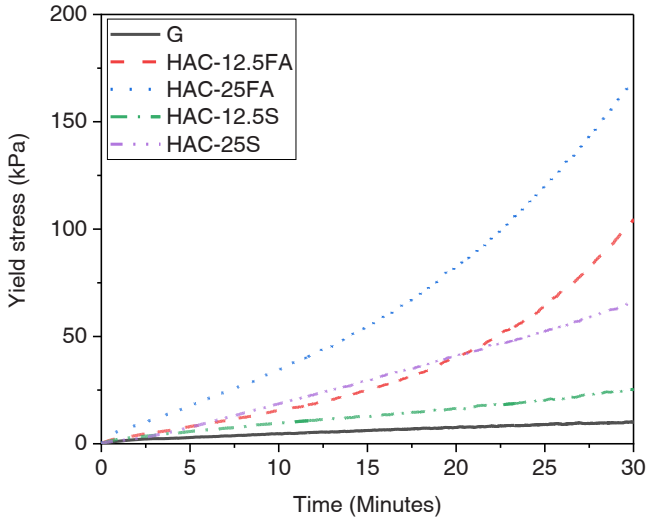

Fig. 7. SYS development of various HAC mixes with time.

yield stress development in the short period even in the presence of retarder. For example, the SYS of HAC-12.5FA, HAC-25FA, HAC-12.5 S and HAC-25S were determined as 15.4 kPa, 34.6 kPa, 9.7 kPa and 18.5 kPa at 10 min, while the corresponding SYS at 30 min were determined as 104.4 kPa, 168.9 kPa, 25.2 kPa and 66.0 kPa, respectively. The rapid development of SYS in these mixes demonstrates the significant enhancement in buildability, which is beneficial for 3D printing.

The comparison of SYS development between different HAC mix groups reveals that the replacement of FA with OPC results in a rapid SYS growth in comparison to the corresponding slag replacement counterparts. The replacement of 12.5 % and 25 % FA showed an early SYS of 64 kPa and 120 kPa at 25 min compared to 20 kPa and 52.5 kPa for the similar slag replacement levels, respectively. The mechanisms for accelerated SYS development in different mix compositions can be explained as follows. In HAC mixes, the hydrated products formed at the first stage are a mixture of C-S-H gel, C-A-S-H gel and N-A-S-H gel as a result of the hydration reaction of OPC and geopolymerisation of slag and FA [44,45]. Moreover, the composition of different gels depends on the proportion of precursors and alkali activator concentrations. In the next stage, given that enough Ca and Al are present in the dissolved mix and the pH of the environment is higher than 12, the above formed initial gels transform into three-dimensional structural gels of C-A-S-H and (N, C)-A-S-H with high degree of polymerisation and increased Si cross-linking [44]. Among the two supplementary cementitious materials of FA and slag, slag has higher degree of dissolution in alkali environment than FA at the ambient temperature [46] and therefore, the presence of high amounts of slag accelerates the early dissolution of CaO, silica and alumina from the precursors, thus showing faster SYS development in comparison to the mixtures containing FA. This is the primary reason for rapid early SYS development in HAC mixes replacing FA compared to the HAC mixes in which slag was replaced. On the other hand, the faster SYS development with the OPC content can be explained by the proportionally increased heat of hydration of OPC, which accelerates the alkali activation of SCMs [32,45].

4.2. Modulus of elasticity of 3D printed specimens at early age

The buildability enhancement in 3D printable mixes must show adequate SYS to overcome the plastic collapse, and high stiffness to prevent the elastic buckling failure. Therefore, the modulus of elasticity of 3D printed HAC mixes was determined with varying time as shown in Fig. 8. It is worth mentioning here that the test was started 10 min after the printing of specimens to allow sufficient time for arranging the experimental setup. The control mix (G) showed steady growth in the elastic modulus due to the geopolymerisation process. The HAC mixes, on the other hand, showed significantly higher elastic modulus at 10 min followed by its significant increase for HAC-FA mixes and a gradual increase for HAC-S mixes, respectively. For instance, the elastic modulus measured at 10 min for G, HAC-12.5FA, HAC-25FA, HAC-12.5 S and HAC-25S was 154 kPa, 490 kPa, 638 kPa, 532 kPa and 624 kPa, respectively. At 20 min, these mixes showed the elastic modulus of 257 kPa, 854 kPa, 1123 kPa, 797 kPa and 941 kPa, respectively. The elastic modulus for HAC-12.5FA and HAC-25FA mixes at 40 min were 1363 kPa and 1797 kPa, respectively, which is much higher than the elastic modulus reported for other mix groups as well as reported in previous studies [47–50]. The high elastic modulus of HAC-FA mixes along with the rapid SYS development can be beneficial in 3DCP for preventing the elastic buckling and plastic collapse failures, respectively, thus enabling the printing of large structures at a high print speed without intermediate stoppings.

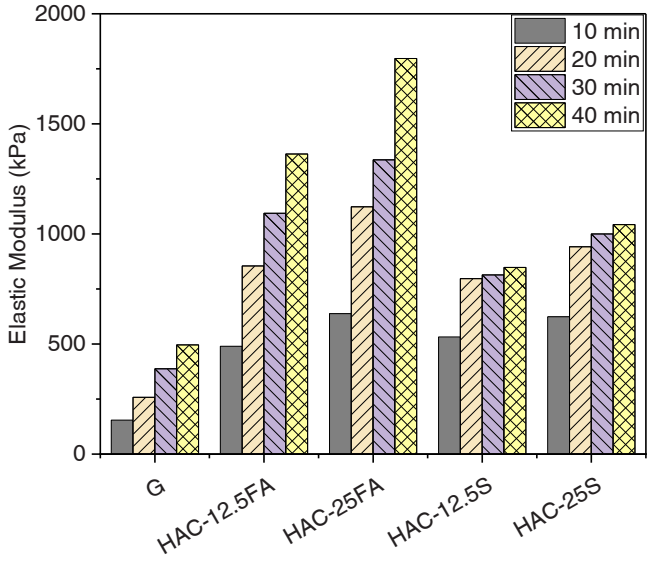

Fig. 8. Elastic modulus development of various HAC mixes with time.

4.3. Setting times of HAC mixes

The initial and final setting of different mix groups, measured by a Vicat apparatus, is depicted in Fig. 9. The setting time measurements provide a direct comparison of the setting rate of HAC mixes, compared to geopolymer concrete. As can be seen from Fig. 9, the control 3D printable mix showed initial and final setting times of 45 min and 62 min respectively, which suggests adequate open time of the mix for pumping and extrusion before placement. On the other hand, all HAC mixes showed the initial setting time of 10–20 min and the final setting times of 19–36 min. It must be underlined that the short setting times of HAC mixes are caused by the reaction of OPC with the alkaline activators, which occurs after printhead mixing. Therefore, the short setting times of these mixes will not interfere with the open time required for pumping and extrusion purposes. Among the different HAC mixes, HAC-12.5FA and HAC-25FA mixes showed comparably short initial setting times of 12 min and 10 min, respectively. This is in good agreement with the SYS measured for all mixes, where these two mixes showed more rapid SYS development compared to other mixes.

In HAC mixes, the introduction of OPC in the alkali activators accelerates the reaction rates of Ca^{2+} ions that are readily available in OPC [51,52]. Furthermore, the exothermic reaction of OPC generates heat which simultaneously accelerates the geopolymerisation process. It was also reported that the reaction rates can be further accelerated by increasing the OPC content in the HAC mixes [53]. This is clearly

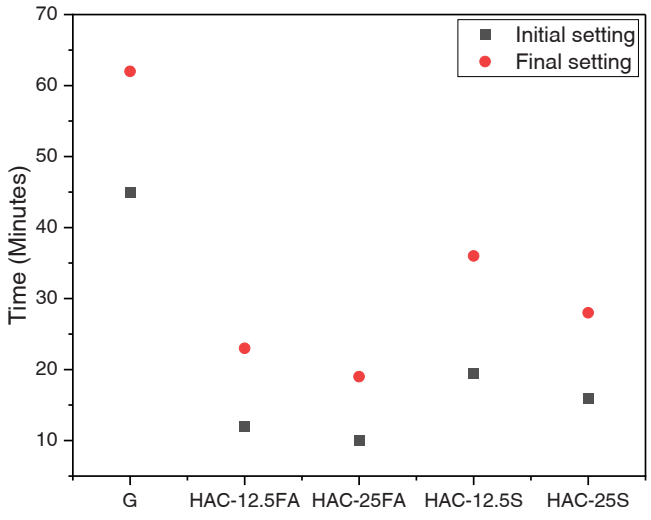

Fig. 9. Initial and Final setting times of HAC mixes.

evident in the studied mixes such that the 25 % OPC replacement levels (HAC-25FA and HAC-25S) showed further reduction in initial and final setting times, compared to their 12.5 % replacement counterparts respectively (HAC-12.5FA and HAC-12.5 S). The short setting times can be beneficial in printhead mixing process to rapidly enhance the SYS and stiffness due to accelerated reaction rates. However, significantly high reaction rates associated with the flash setting of OPC can lead to weak interlayer bond strength if the print cycle time is higher than setting times. In this regard, the hydration setting behaviour of HAC can be delayed by using the retarders such as glucose, sucrose, borax, sodium gluconate, etc. [33,54]. The dosage of the retarders can be chosen to increase the setting time above the cycle time of printing process while showing an adequate SYS development for buildability.

4.4. Viscosity recovery of HAC mixes

The viscosity recovery of printable mixes after the printhead mixing process is depicted in Fig. 10. As can be seen, the apparent viscosity of printable mixes after re-shearing process is reduced to a minor extent, compared to the apparent viscosity prior to the high shear mixing process (i.e., stage 2 mixing). For instance, the apparent viscosity of G, HAC-12.5FA, HAC-12.5 S and HAC-25S measured prior to the re-shearing was $\sim 2.3\times10^5$, $\sim 1.6\times10^5$, $\sim 8.7\times10^4$, $\sim 4.3\times10^4$, respectively. The corresponding apparent viscosity after the re-shearing process was $\sim 2.3\times10^4$, $\sim 1.5\times10^4$, $\sim 8.1\times10^4$ and $\sim 4.8\times10^4$, respectively. The comparison of apparent viscosity before and after re-shearing process indicates that the mixes subjected to the re-shearing process will not significantly change the apparent viscosity. Therefore, the extrudability of the studied mixes were not affected by re-shearing process. This observation guarantees that the excessive mixing in the printhead will not significantly change the extrudability and shape retention properties of concrete. On the other hand, the comparison of apparent viscosity between different mix groups indicates that the mixes replacing FA (HAC-12.5FA and HAC-25FA) have higher apparent viscosity than the mixes replacing slag (HAC-12.5 S and HAC-25S). The control mix showed lowest apparent viscosity in comparison to all other mix groups. This is in good agreement with the SYS development of printable mixes, where HAC-FA group mixes showed rapid early SYS development compared to other mix groups. It should be noted that the apparent viscosity of HAC-25FA mix could not be measured since the apparent viscosity of this mix exceeded the limit of the Viskomat rheometer. The maximum torque of a Viskomat XL rheometer is 5000 Nm and the HAC-25FA mix requires more torque to shear the sample and therefore, the rheometer cannot be used.

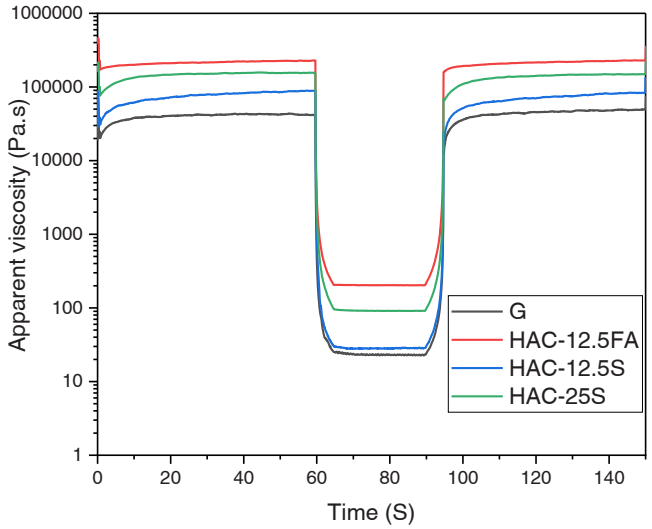

Fig. 10. Viscosity recovery of HAC mixes.

4.5. Compressive strength of 3D printed concrete

The compressive strength of mould-cast and 3DCP specimens at three orthogonal directions at the age of 7 and 28 days are presented in Fig. 11. The comparison of mould-cast specimens suggests that the HAC mixes with the slag replacement (HAC-12.5S and HAC-25S) have lower compressive strength than the control geopolymer mix. The reduction in compressive strength for these mixes could be attributed to the higher water-to-binder ratio than control mix group, thus reducing the compressive strength at both ages. The high water-to-binder ratio was chosen to attain the printability properties of concrete. In addition, these two mix groups contain higher proportion of fly ash than slag compared to the control mix. FA is a low calcium content precursor compared to slag that leads to lower reactivity than the calcium rich precursor of slag and forms products which are Ca deficient such as N-A-S-H and C-A-S-H.

On the other hand, the HAC mixes formulated by replacing fly ash (HAC-12.5FA and HAC-25FA) showed higher compressive strength than the control mix even at high water-to-binder ratio. The compressive strength determined for G, HAC-12.5FA and HAC-25FA mix groups for mould-cast specimens were 44.45 MPa, 47.61 MPa and 50.67 MPa at 7 days followed by further strength development at 28 days to 58.83 MPa, 63.17 MPa and 70.6 MPa, respectively. The significant strength enhancement at both ages for HAC mixes replacing the FA with OPC can be explained as the comparably high Ca/Si ratio that leads to the formation of C-S-H and C-A-S-H at a larger proportion. They assist in filling the voids in the microstructures leading to a more refined and densified microstructure. This is more pronounced in the HAC-25FA mix, where the compressive strength is even higher at a higher water-to-binder ratio compared to control mix and HAC-12.5FA mix.

It is interesting to note that the 3D printed specimens showed a lower compressive strength than the corresponding mould-cast specimens along with anisotropic behaviour of compressive strength properties. The anisotropic behaviour of 3D printed specimens, demonstrating the highest compressive strength in the longitudinal direction and least compressive strength in lateral direction, is primarily due to the extrusion pressure in the longitudinal direction leading to highest compaction and the existence of interlayer in the failure plane of lateral direction causing least strength properties, respectively. This trend agrees with the past studies, where the anisotropic compressive strength properties were reported for 3D printed specimens with the strength values in the decreasing order for longitudinal, perpendicular, and lateral directions [55,56].

Furthermore, the reduced compressive strength of 3D printed specimens, compared to mould-cast specimens, can be explained by the large void volume content in 3D printed specimens due to the nature of fabrication. The 3D printing process is a layer-wise material deposition, where the interlayer porosity is unavoidable in addition to the intra-layer porosity. In the mould-cast fabrication, the monolithic cast process eliminates the large amount of void content primarily due to the compaction and the absence of discrete layers. This can be validated by comparing the void volume percentage determined by the AVPV test as shown in Fig. 12. Regardless of the mix group, 3D printed samples showed higher permeable void volume than the mould-cast specimens. For example, the AVPV determined for control geopolymer mix (G) was 14.7 % and 18.0 % for mould-cast and 3D printed specimens, respectively, whereas the corresponding AVPV for HAC-25FA mix were 10.6 % and 14.5 %, respectively. It is also noted that the AVPV trend follows the compressive strength results. The highest AVPV was observed for HAC-12.5 S and the lowest one was for HAC-25FA. These results support the formation of compact and densified microstructure in HAC-25FA mixes that resulted in the highest compressive strength properties, whereas the HAC-12.5 S has a less densified microstructure causing the lowest compressive strength.

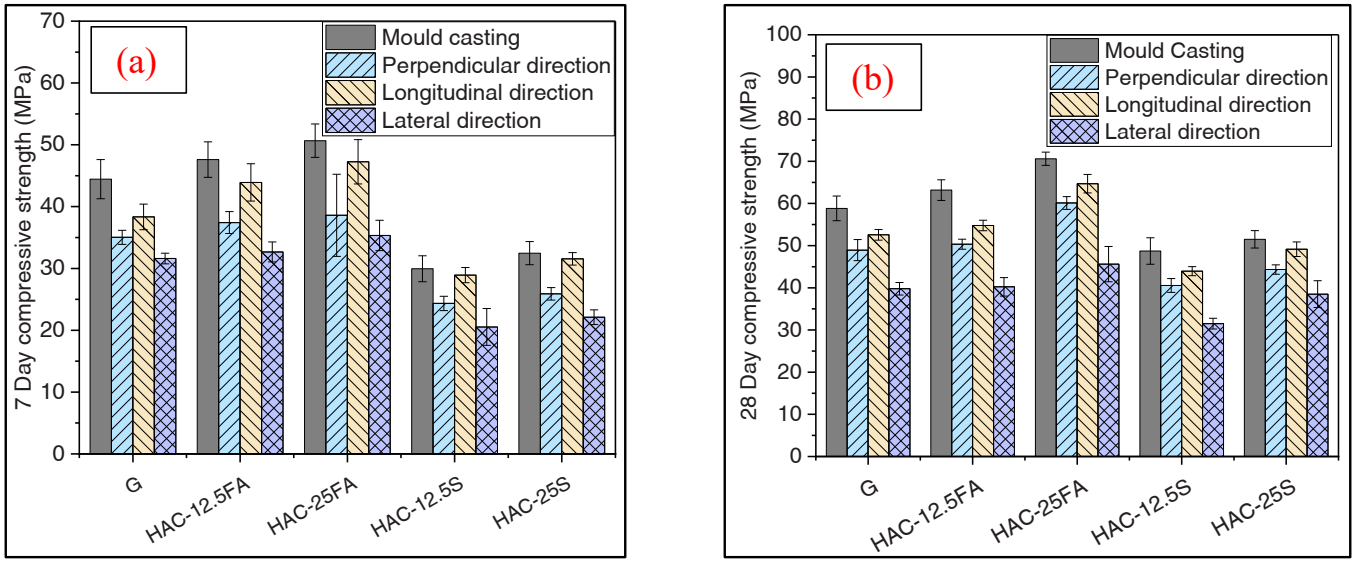

Fig. 11. Directional compressive strength of HAC mixes at (a) 7 days and (b) 28 days (Error bars indicate average ± one standard deviation).

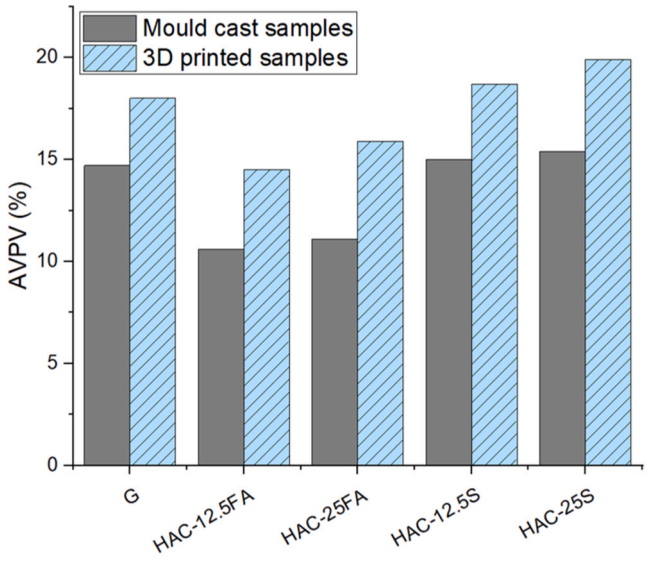

Fig. 12. Apparent volume of permeable voids (AVPV) of mould casting and 3D printed HAC mixes.

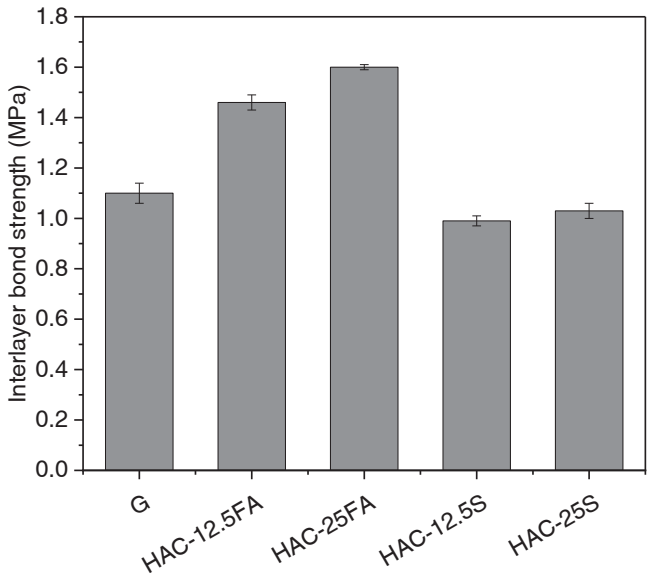

Fig. 13. Interlayer bond strength of 3D printed HAC samples at 28 days (Error bars indicate average ± one standard deviation).

4.6. *Interlayer bond strength of 3D printed concrete*

Fig. 13 shows the interlayer bond strength of 3D printed specimens determined at 28 days of age by following a direct tensile test for interlayer bond. The interlayer bond strength follows a similar trend to the compressive strength test results, where significantly higher bond strength was observed for the HAC mixes replacing FA with OPC (HAC-12.5FA and HAC-25FA) and the lowest bond strength values were determined for HAC mixes with slag replacement (HAC-12.5 S and HAC-25S). Moreover, as the OPC replacement level increases, the interlayer bond strength increases for the HAC mixes replacing the FA. This is quite an interesting observation since the interlayer bond strength is primarily governed by the malleability of printed filaments and the surface moisture content. The printable mixes with extended setting time would have enhanced malleability and high surface moisture content compared to rapid setting printable mixes. In this regard, all HAC mixes have rapid setting behaviour with short setting time compared to the control mix. However, the HAC-12.5FA and HAC-25FA mixes showed significantly higher bond strength than other mixes. This can be attributed to the increased matrix strength of these two mixes, compared to other mixes, which led to enhanced physical interlocking at the interlayer due to refined and densified microstructure. Further investigation is necessary to validate the proposed reasons. Nevertheless, the HAC mixes with FA replacement showed enhanced interlayer bond strength properties that can be beneficial for increasing the lateral load carrying capacity of building elements.

4.7. *Microstructural analysis of 3D printed concrete*

The micromorphology of different HAC mixes, observed through an SEM, after 28 days curing age is shown in Fig. 14. The SEM images show that the control specimen (Fig. 14a) has a large number of voids along with the microcracks on the observed surface. The HAC-FA mixes (Fig. 14b and Fig. 14c), on the other hand, have a dense microstructure with least amount of any visible voids and microcracks. Furthermore,

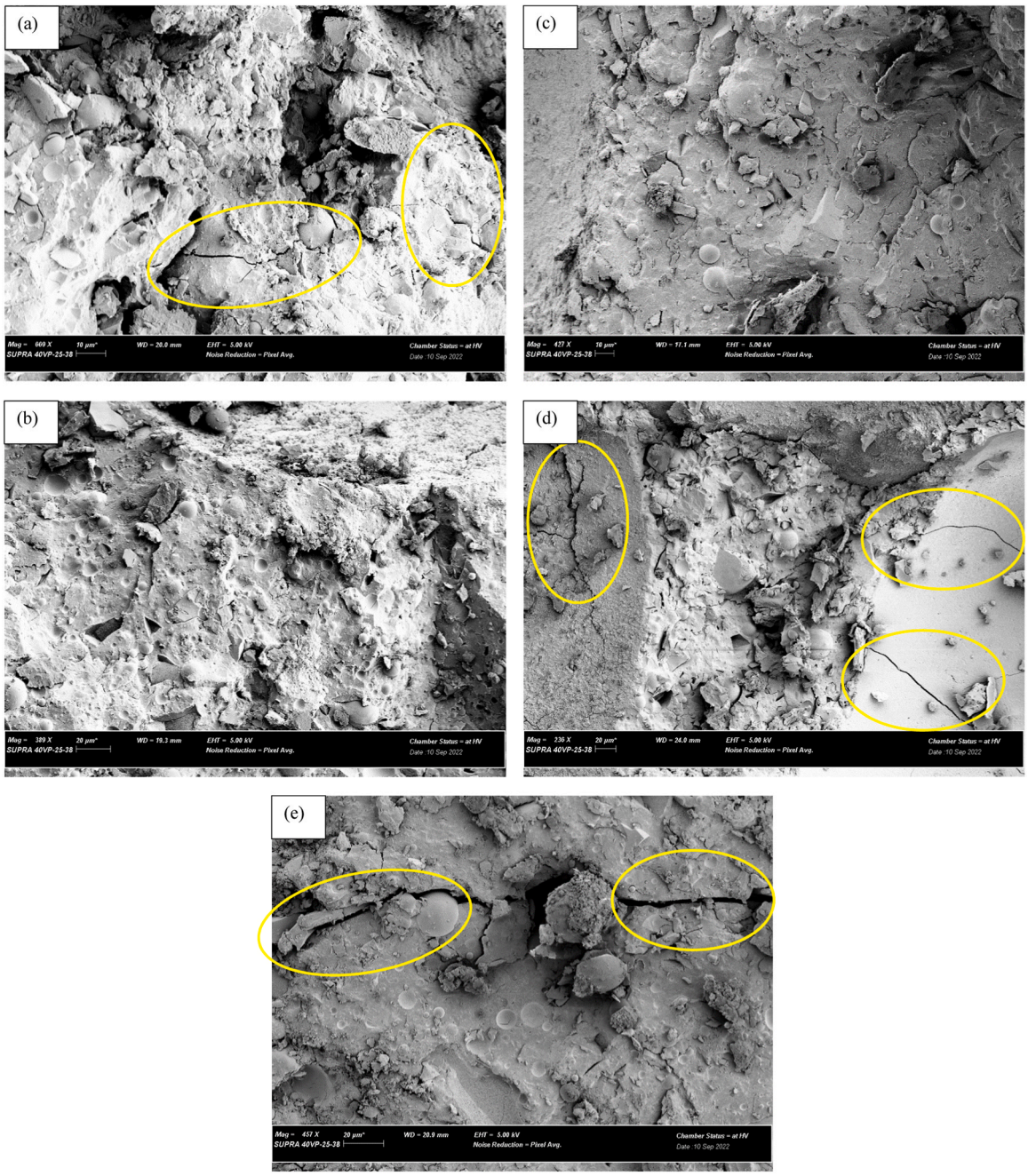

Fig. 14. SEM images of HAC mixes: (a) G; (b) HAC-12.5FA; (c) HAC-25FA; (d) HAC-12.5 S; (e) HAC-25S.

the formation of deep microcracks and voids is evident in the HAC-S specimens (Fig. 14d and Fig. 14e). This reveals that the control and HAC-S groups have a less dense microstructure along with the formation of microcracks compared to the HAC-FA mix groups. This observation well agrees with the AVPV test results presented in Section 4.5, where the apparent volume of permeable voids of HAC-FA mixes was lower than other mix groups.

5. Conclusions

This study investigated the printhead mixing of two-part components to develop a printable hybrid alkali activated cement (HAC) mixes for the emerging concrete 3D printing applications. The two-part slurry blends containing geopolymer slurry and OPC slurry as two components were subjected to short duration printhead mixing process. The fresh and hardened properties of resultant printable mixes were studied. Based on the results obtained, the following conclusions can be drawn:

1. The HAC mixes replacing FA with OPC at 12.5 % and 25 % showed significantly faster early age static yield strength (SYS) development and higher modulus of elasticity compared to the HAC mixes with similar replacement levels of slag.
2. The measured SYS and modulus of elasticity for HAC-25FA mix were 17 times and 3.5 times higher than the respective properties observed for control specimens at 30 min, demonstrating its significantly enhanced buildability.
3. The extrudability of the printable mixes assessed by a viscosity recovery test indicates that all mix groups have fully recovered the apparent viscosity after the re-shearing process. This suggests that

the secondary mixing at the print head will not affect the extrudability and shape retention of the printed layers.
4. The hardened properties of compressive strength and interlayer bond strength of 3D printed specimens showed that the HAC-FA mixes yielded higher strength values while the HAC-S mixes showed reduced strengths. The strength reduction in HAC-S mixes can be attributed to high water-to-binder ratio as well as the formation of a large amounts of N-A-S-H gels compared to C-A-S-H and C-S-H gels primarily formed in other mix groups.
5. The microstructural analysis reveals that the control and HAC-S mixes have a less dense microstructure with large void content and microcracks compared to HAC-FA mixes where these defects were least present.

CRediT authorship contribution statement

Sayanthan Ramakrishnan: Writing – original draft, Methodology, Investigation, Conceptualization. **Kirubajiny Pasupathy:** Writing – review & editing, Visualization, Methodology, Formal analysis. **Viktor Mechtcherine:** Writing – review & editing, Visualization, Validation, Supervision, Conceptualization. **Jay Sanjayan:** Writing – review & editing, Validation, Supervision, Resources, Methodology, Conceptualization.

Declaration of Competing Interest

The authors declare that they have no known competing financial interests or personal relationships that could have appeared to influence the work reported in this paper.

Data Availability

Data will be made available on request.

Acknowledgements

The authors acknowledge the Digital Construction and Smart Structures Laboratories at Swinburne University of Technology and the Australian Research Council (DE190100646) for supporting this work.

References

[1] F. Bos, et al., Additive manufacturing of concrete in construction: potentials and challenges of 3D concrete printing, Virtual Phys. Prototyp. 11 (3) (2016) 209–225.
[2] M.K. Mohan, et al., Extrusion-based concrete 3D printing from a material perspective: a state-of-the-art review, Cem. Concr. Compos. 115 (2021) 103855.
[3] R.A. Buswell, et al., 3D printing using concrete extrusion: a roadmap for research, Cem. Concr. Res. 112 (2018) 37–49.
[4] G. De Schutter, et al., Vision of 3D printing with concrete — technical, economic and environmental potentials, Cem. Concr. Res. 112 (2018) 25–36.
[5] V. Mechtcherine, et al., Extrusion-based additive manufacturing with cement-based materials – production steps, processes, and their underlying physics: a review, Cem. Concr. Res. 132 (2020) 106037.
[6] Y. Tao, et al., Stiffening controllable concrete modified with redispersible polymer powder for twin-pipe printing, Cem. Concr. Res. 161 (2022) 106953.
[7] Y. Weng, et al., Investigation of interlayer adhesion of 3D printable cementitious material from the aspect of printing process, Cem. Concr. Res. 143 (2021) 106386.
[8] W. Lao, M. Li, T. Tjahjowidodo, Variable-geometry nozzle for surface quality enhancement in 3D concrete printing, Addit. Manuf. 37 (2021) 101638.
[9] N. Roussel, Rheological requirements for printable concretes, Cem. Concr. Res. 112 (2018) 76–85.
[10] S. Muthukrishnan, S. Ramakrishnan, J. Sanjayan, Technologies for improving buildability in 3D concrete printing, Cem. Concr. Compos. 122 (2021) 104144.
[11] A.S. Suiker, et al., Elastic buckling and plastic collapse during 3D concrete printing, Cem. Concr. Res. 135 (2020) 106016.
[12] R.J.M. Wolfs, A.S.J. Suiker, Structural failure during extrusion-based 3D printing processes, Int. J. Adv. Manuf. Technol. 104 (1) (2019) 565–584.
[13] Y. Tao, et al., Development of a calcium sulfoaluminate-Portland cement binary system for twin-pipe 3D concrete printing, Cem. Concr. Compos. 138 (2023) 104960.
[14] Esnault, V., et al. Experience in online modification of rheology and strength acquisition of 3D printable mortars. in RILEM International Conference on Concrete and Digital Fabrication. 2018. Springer.
[15] Meijde, G.Y.G.Vd, Accelerating early strength and stiffness development of a portland cement-based mortar for 3D printing, in built environment. 2019, TU/E Eindhoven.
[16] C. Gosselin, et al., Large-scale 3D printing of ultra-high performance concrete – a new processing route for architects and builders, Mater. Des. 100 (2016) 102–109.
[17] E. De Lena, et al., Techno-economic analysis of calcium looping processes for low CO2 emission cement plants, Int. J. Greenh. Gas. Control 82 (2019) 244–260.
[18] T.A. Santos, M.S. Cilla, and e.D.V. Ribeiro, Use of asbestos cement tile waste (ACW) as mineralizer in the production of Portland cement with low CO2 emission and lower energy consumption, J. Clean. Prod. 335 (2022) 130061.
[19] V. Sousa, J.A. Bogas, Comparison of energy consumption and carbon emissions from clinker and recycled cement production, J. Clean. Prod. 306 (2021) 127277.
[20] S. Nie, et al., Analysis of theoretical carbon dioxide emissions from cement production: methodology and application, J. Clean. Prod. 334 (2022) 130270.
[21] P. Duxson, et al., Geopolymer technology: the current state of the art, J. Mater. Sci. 42 (9) (2007) 2917–2933.
[22] P. Duxson, et al., The role of inorganic polymer technology in the development of 'green concrete, Cem. Concr. Res. 37 (12) (2007) 1590–1597.
[23] S. Muthukrishnan, S. Ramakrishnan, J. Sanjayan, Set on demand geopolymer using print head mixing for 3D concrete printing, Cem. Concr. Compos. 128 (2022) 104451.
[24] S. Muthukrishnan, S. Ramakrishnan, J. Sanjayan, In-line activation of geopolymer slurry for concrete 3D printing, Cem. Concr. Res. 162 (2022) 107008.
[25] Y. Tao, et al., Blending performance of helical static mixer used for twin-pipe 3D concrete printing, Cem. Concr. Compos. 134 (2022) 104741.
[26] Y. Tao, et al., Twin-pipe pumping strategy for stiffening control of 3D printable concrete: From transportation to fabrication, Cem. Concr. Res. 168 (2023) 107137.
[27] Y. Tao, et al., Mechanical and microstructural properties of 3D printable concrete in the context of the twin-pipe pumping strategy, Cem. Concr. Compos. 125 (2022) 104324.
[28] K. Pasupathy, S. Ramakrishnan, J. Sanjayan, Effect of hydrophobic surface-modified fine aggregates on efflorescence control in geopolymer, Cem. Concr. Compos. 126 (2022) 104337.
[29] A. Palomo, et al., Opc-fly ash cementitious systems: study of gel binders produced during alkaline hydration, J. Mater. Sci. 42 (9) (2007) 2958–2966.
[30] H. Ye, et al., Understanding the drying shrinkage performance of alkali-activated slag mortars, Cem. Concr. Compos. 76 (2017) 13–24.
[31] H.E. El-Yamany, M.A. El-Salamawy, N.T. El-Assal, Microstructure and mechanical properties of alkali-activated slag mortar modified with latex, Constr. Build. Mater. 191 (2018) 32–38.
[32] L. Xue, Z. Zhang, H. Wang, Hydration mechanisms and durability of hybrid alkaline cements (HACs): a review, Constr. Build. Mater. 266 (2021) 121039.
[33] A.K. Mohapatra, B. Pradhan, Hybrid alkali activated cements (HAACs) system: a state-of-the-art review on fresh, mechanical, and durability behaviour, Constr. Build. Mater. 361 (2022) 129636.
[34] Zealand, A.S.N. and Committee BD-031, Supplementary cementitious materials Part 1: Fly ash, in AS/NZS 3582.1:2016. 2016.
[35] Standard, A., General purpose and blended cements. Standard, Standard Australia, 2010.
[36] L.N. Assi, E.E. Deaver, P. Ziehl, Using sucrose for improvement of initial and final setting times of silica fume-based activating solution of fly ash geopolymer concrete, Constr. Build. Mater. 191 (2018) 47–55.
[37] U. Rattanasak, K. Pankhet, P. Chindaprasirt, Effect of chemical admixtures on properties of high-calcium fly ash geopolymer, Int. J. Miner. Metall. Mater. 18 (2011) 364–369.
[38] K. Pasupathy, S. Ramakrishnan, J. Sanjayan, 3D concrete printing of eco-friendly geopolymer containing brick waste, Cem. Concr. Compos. (2023) 104943.
[39] Z. Chang, et al., A review of methods on buildability quantification of extrusion-based 3D concrete printing: From analytical modelling to numerical simulation, Dev. Built Environ. 16 (2023) 100241.
[40] S. Muthukrishnan, S. Ramakrishnan, J. Sanjayan, Effect of alkali reactions on the rheology of one-part 3D printable geopolymer concrete, Cem. Concr. Compos. 116 (2021) 103899.
[41] S. Ramakrishnan, et al., Concrete 3D printing of lightweight elements using hollow-core extrusion of filaments, Cem. Concr. Compos. 123 (2021) 104220.
[42] S. Hou, et al., A review of 3D printed concrete: performance requirements, testing measurements and mix design, Constr. Build. Mater. 273 (2021) 121745.
[43] T. Marchment, J. Sanjayan, M. Xia, Method of enhancing interlayer bond strength in construction scale 3D printing with mortar by effective bond area amplification, Mater. Des. 169 (2019) 107684.
[44] L. Xue, Z. Zhang, H. Wang, Early hydration kinetics and microstructure development of hybrid alkali activated cements (HAACs) at room temperature, Cem. Concr. Compos. 123 (2021) 104200.
[45] I. García-Lodeiro, A. Fernández-Jiménez, A. Palomo, Variation in hybrid cements over time. Alkaline activation of fly ash–portland cement blends, Cem. Concr. Res. 52 (2013) 112–122.
[46] S. Puligilla, P. Mondal, Role of slag in microstructural development and hardening of fly ash-slag geopolymer, Cem. Concr. Res. 43 (2013) 70–80.
[47] R.J.M. Wolfs, F.P. Bos, T.A.M. Salet, Early age mechanical behaviour of 3D printed concrete: numerical modelling and experimental testing, Cem. Concr. Res. 106 (2018) 103–116.
[48] B. Panda, J.H. Lim, M.J. Tan, Mechanical properties and deformation behaviour of early age concrete in the context of digital construction, Compos. Part B: Eng. 165 (2019) 563–571.

[49] R.J.M. Wolfs, F.P. Bos, T.A.M. Salet, Triaxial compression testing on early age concrete for numerical analysis of 3D concrete printing, Cem. Concr. Compos. 104 (2019) 103344.
[50] Z. Chang, et al., Numerical simulation of elastic buckling in 3D concrete printing using the lattice model with geometric nonlinearity, Autom. Constr. 142 (2022) 104485.
[51] P. Nath, P.K. Sarker, Use of OPC to improve setting and early strength properties of low calcium fly ash geopolymer concrete cured at room temperature, Cem. Concr. Compos. 55 (2015) 205–214.
[52] P. Chindaprasirt, et al., Effect of calcium-rich compounds on setting time and strength development of alkali-activated fly ash cured at ambient temperature, Case Stud. Constr. Mater. 9 (2018) e00198.
[53] M. Askarian, et al., Mechanical properties of ambient cured one-part hybrid OPC-geopolymer concrete, Constr. Build. Mater. 186 (2018) 330–337.
[54] W. Rakngan, et al., Controlling workability in alkali-activated Class C fly ash, Constr. Build. Mater. 183 (2018) 226–233.
[55] Q. Jiang, et al., Modification effect of nanosilica and polypropylene fiber for extrusion-based 3D printing concrete: Printability and mechanical anisotropy, Addit. Manuf. 56 (2022) 102944.
[56] B. Panda, S. Chandra Paul, M. Jen Tan, Anisotropic mechanical performance of 3D printed fiber reinforced sustainable construction material, Mater. Lett. 209 (2017) 146–149.